~~Supervision of~~ seismic velocity models of the Reykjanes Peninsula Rift, SW Iceland

Bohuslav Růžek,[1] Jana Doubravová,[1] and Josef Horálek [1,†]

[1]Institute of Geophysics CAS, Boční 1401/II, 141 31 Prague 4, Czech Republic

5   [†]Deceased

Correspondence to: Bohuslav Růžek (b.ruzek@ig.cas.cz)

In memory of Josef Horálek, 1948 - 2023

Abstract. Most methods for processing seismological data require a suitable velocity model characteristic for the given region being defined. This is also the case of the Reykjanes Peninsula (RP) in SW Iceland, where the REYKJANET seismic

10   network was built to monitor local seismicity in the rift zone. At present, four previously published 1D velocity models (SIL, BRA, TRY and VOG) can potentially be used, ~~prompting us to determine which one is the best. In order to address this issue,~~ we arranged a contest ~~in which all four 1D models and one additional 3D model (T3D) were entered.~~ Uniform methodology for classifying the models was applied and included an analysis of: (i) post-localization travel-time residuals, (ii) residuals of the P-wave first-motion incidence angle and (iii) model-predicted and measured Rayleigh-wave dispersion.

15   We discovered that no single model was unequivocally the most optimal, as the differences between them proved rather minor. A common shortcoming of all the models is the bias of the P-wave first motion incidence angle residuals, which may be a general problem for methods working with P-wave amplitudes (e.g., moment tensor solutions). The VOG model was selected with a weak preference.

~~Finally,~~ we propose a simple method for modifying ~~any of~~ the 1D models by adding a station-dependent surface layer with a

20   vertical velocity gradient. This way, a pseudo-3D model is generated which is fully competitive with a true 3D model while retaining the simplicity of 1D ray tracing. The efficiency of this correction was demonstrated using the VOG model. The corrected VOG model provides post-localization residuals comparable with the true 3D model T3D, has zero bias in predicting the P-wave first-motion incidence angles, and agrees acceptably in predicting the Rayleigh-wave phase-velocity known from other sources. While calculations with a 3D model can be clumsy, the proposed pseudo-3D model is defined by

25   ~~few parameters and is very easy to use.~~ Its applicability is limited to earthquake sources deeper than the deepest lower limit of the topmost layer below the stations.

1 Introduction

Iceland is undoubtedly a highly attractive locality for many geoscience disciplines. The Mid-Atlantic Ridge, one of the most prominent geological regions in the world, reaches the Earth's surface there and allows for direct observation and measurement. In addition to fundamental research, geoscience investigations also have a big impact on a wide range of industrial applications and on the real life of the population (geothermal power plants and heating, volcanic monitoring).

The Institute of Geophysics (IG) and Institute of Rock Structure and Mechanics (IRSM) of the Czech Academy of Sciences, Czech Republic, in cooperation with the Iceland Geosurvey (ISOR) in Reykjavík, Iceland, and Charles University in Prague, have been operating the REYKJANET seismic network since 2013 on the Reykjanes Peninsula, see Fig.1 and www2023a. The network consists of 15 broadband seismic stations providing data in real time. The processing of seismic data requires the identification an appropriate seismic velocity model. Over the decades, great efforts have been made in the determination of velocity models (Bjarnason et al., 1993; Weir et al., 2001; Tryggvason et al., 2002; Vogfjörd et al., 2002; Brandsdóttir et al.,
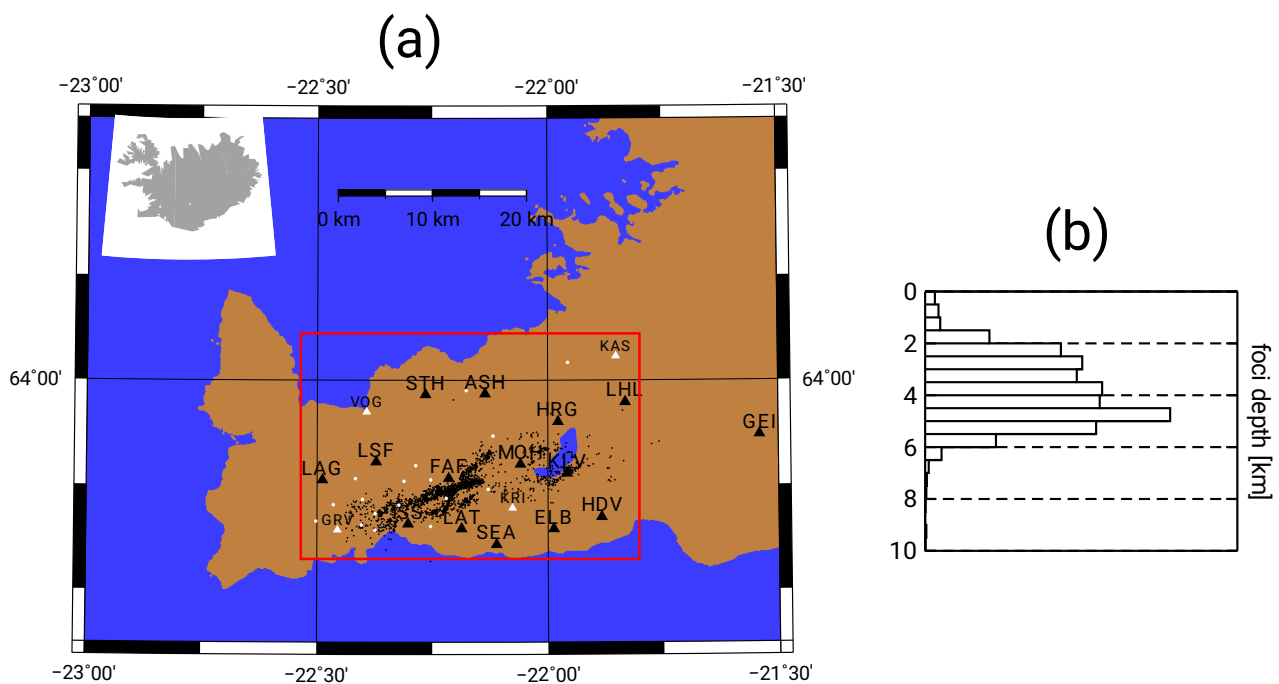

Figure 1. (a) A map showing 15 REYKJANET stations (black triangles with station codes in bold). The red rectangle indicates the region for which the supervised models are considered. One REYKJANET station (GEI) is located outside the rectangle and is not included in this study. In 2023, several permanent stations of the SIL network (smaller white rectangles with station codes in italics) were available as well as around 20 temporary stations operated by Cambridge University (small white circles without codes). The results of this study are based solely on data provided by the REYKJANET stations. Earthquake epicentres represented by small black dots are distributed along prolonged structures, which may be a subject of special interest, though it is not discussed in this paper. **(b) Depth distribution of hypocentres in the form of a histogram. Predominantly shallow earthquakes with a depth range of ~ 2 - 6 km are observed.**

2008; Geoffroy and Dorbath, 2008; Mitchell et al., 2013; Greenfield et al., 2016; Jousset et al., 2016; Málek et al., 2019; Růžek, 2021). ~~These models differ in many aspects~~ (yielding only P or both P and S velocities; different model resolution;

40   different depth range and regional extent; 1D, 2D or 3D model geometry), prompting the question as to which is most suitable for a given application.

The goal of this paper is not to construct a completely new velocity model or to extend the already long list of available models. Instead, the goal is to test several already published velocity models that are used at IG for data processing and to identify any potential weak points in order to select the best model. Additionally, we tried to calculate a small velocity

45   correction which could further improve the performance of the preferred model. This correction is based on: a) fitting the P- and S-wave travel-times (similarly to local earthquake tomography); (b) fitting observed and predicted P-wave polarizations and c) fitting the Rayleigh-wave phase-velocity dispersion. To ~~calculate the corrected model, a medium sized inverse problem was solved and the resulting (corrected) velocity model was re-evaluated.~~ The model is built up as a station-dependent 1D isotropic model which means it can be classified as an efficient "pseudo-3D" model that is easy to use.

50   **2 Velocity models**

Different velocity models have already been tested by Jakoubková (2018), who discussed the impact of the velocity model on hypocentre localization; the REYKJANET stations and the voluminous bulletin of local earthquakes were used for the tests. In our study, we test the same set of four models as Jakoubková (2018) (models SIL, VOG, TRY and BRA); in addition, we test a 3D tomographic model (T3D), which is a simple isotropic projection of a rather complex inhomogeneous anisotropic

55   model calculated earlier by Růžek (2021). The original specification of these five models is different. In order to guarantee fair testing and uniform comparison, all of the models were transformed (Jakoubková, 2018, Appendix A.) into 1D piecewise linear continuous functions of depth, which is the most common form used for representing velocity models. Model T3D was tested both in its original 3D and simplified 1D representations. In summary, our testing suite includes:

- SIL, developed by Bjarnason et al. (1993) and currently used for automated event location in SW Iceland, including
60   the Reykjanes peninsula;
- VOG, published by Vogfjörd et al. (2002);
- TRY, calculated using 3D seismic tomography (Tryggvason et al., 2002);
- BRA, Brandsdóttir et al. (2008);
- T3D, an isotropic projection of the 3D anisotropic model published by Růžek (2021).

65   The reason for our choice is that the first four models have long been used at IG, primarily for hypocentre localization, with good results. Moreover, the TRY model covers the entirety of the REYKJANET network. Model T3D was included in order to ascertain the added value of using much more complex velocity models with numerous parameters instead of simple 1D models. For a graphical representation of the velocity models, see Fig.2., numerical specifications can be found in Appendix A. An obvious drawback of T3D is the absence of a low-velocity surface zone, which can be attributed to the quality of data

70   that was used to calculate the model by Růžek (2021): only earthquake data were available and there were no surface sources (e.g. explosions). This means that the surface part of T3D is of formal importance and is presented only for the completeness of the models. All five models, starting from a depth of ~2 km, are quite similar.
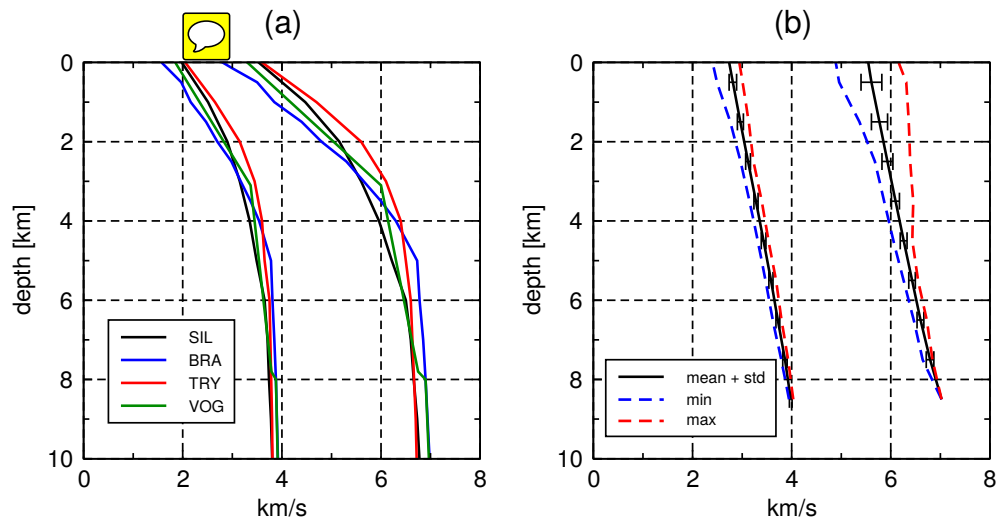

Figure 2. Five velocity models tested in this paper. The depth range of all models is limited to 10 km due to the limited depth of the earthquakes used for testing. (a) 1D velocity models considered as piecewise linear functions of depth. Note that the model TRY is a 1D projection of an originally 3D velocity model. (b) 3D tomographic model T3D schematically shown as a depth-dependent velocity distribution averaged along horizontal planes. Together with the mean velocity, standard deviation and extreme values are presented.

2.1 Test of Hypocentre Localization

We ~~have actually~~ replicated the work of Jakoubková (2018), ~~though we did include~~ one additional model (T3D) and ~~used~~ a

75   bigger localization data set. We used the localization software NonLinLoc by Lomax et al. (2009; www2023b), to obtain the hypocentre co-ordinates, post-localization travel-time residuals and station corrections. ~~Regarding the localized earthquake data,~~ 2541 events were included, covering the time period Sept. 2013 - Nov. 2021. The number of phases was 213 for P-waves and 28571 for S-waves. ~~The map of epicentres, together with REYKJANET stations, is shown in~~ Fig. 1.

First, we calculated the distribution of post-localization travel-time residuals. While the relevance of travel-time residuals as

80   a measure of localization accuracy ~~may spark lengthy debates,~~ this is the first criterion which can be used without the inclusion of any other information. ~~The results are shown in Fig. 3. Let us discuss the 1D models first.~~ All of ~~these~~ models provide similar P-wave residuals close to 0.070 s. Some differences are visible between the S-wave residuals: ~~the best model, VOG, yields 0.102 s while the worst model, TRY, yields 0.118 s. From this point of view, if considering 1D models only, the VOG model should be preferred while TRY should be suppressed.~~ The other two models, SIL and BRA, fall

85   somewhere in between. The 3D model T3D ~~is not tested in order to compete with the 1D models but rather to provide~~ a

"lower limit" of travel-time residuals towards which the 1D models should converge: the P- and S-wave residuals are 0.062 s (= 89% of VOG) and 0.084 s (= 82% of VOG), resp.

Next, we compared hypocentral coordinates (including origin time) by using different models. Each earthquake was
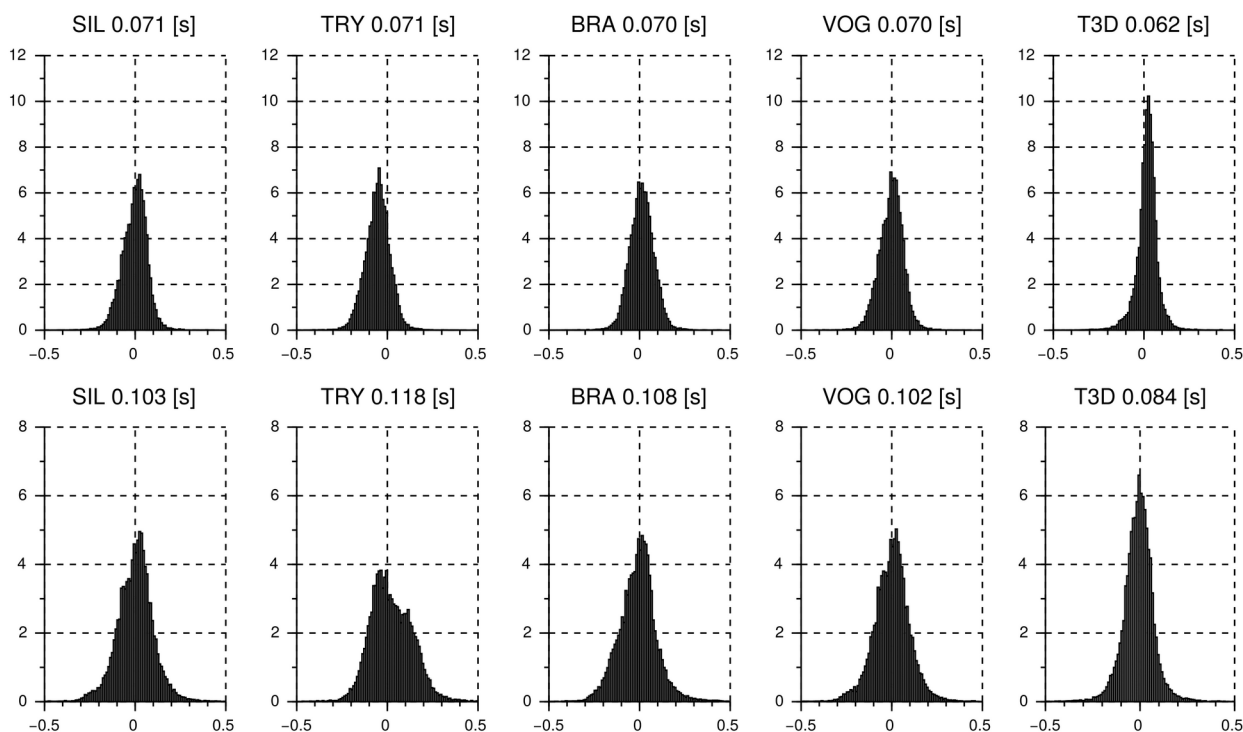

Figure 3. Histograms of P-wave (upper row) and S-wave (lower row) travel-time residuals for different velocity models, ordered according to the P-wave residuals from the worst case in the leftmost position to the best case in the right-most position. The velocity model is indicated above each histogram together with the RMS in seconds. All the histograms are normalized, i.e., the area below each curve is 1.

localized five times using one of the tested models. The average hypocentre and origin time were then evaluated and

90 deviations between "raw" and average hypocentres were recorded. Finally, these deviations were averaged over the set of earthquakes, separately for each tested model. The comparison is visualised in Fig. 4. As expected, the epicentral coordinates are nearly identical regardless of the velocity model. The differences are of the order ~100 m or less and are likely of no practical importance. Greater differences can be observed in the depth of foci. The SIL model provides on average 400 m shallower hypocentres, while models TRY and BRA yield the opposite results, shifting the hypocentres approximately

95 250 m deeper. Note that Jakoubková (2018), using a different data set, arrived at similar conclusions. When inspecting deviations regarding the origin time (Fig. 4b), one can observe a maximum positive shift of 0.2 s for model T3D and minimum negative shift -0.15 s for model BRA, while other velocity models are closer to the average. Similarly, regarding

5

~~the discussion of travel-time residuals,~~ there is no rigorous criterion which could favour one of the models based on the hypocentral deviations from mean values. ==Nevertheless, different authors have constructed their models by neglecting==
100 ==different real world features, which appears to be a rather haphazard process.== In that case, the average model would potentially be the best one. If we accept this premise, the model with the smallest deviations from the average should be preferred. In our case, this would be the VOG model.
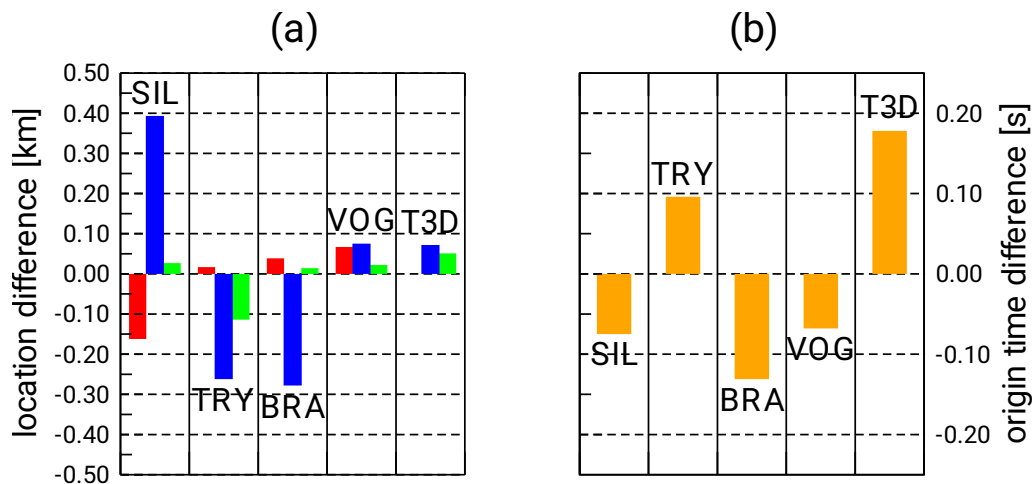

Figure 4. (a) Triplets of average deviations of hypocentre coordinates in E-W (red), N-S (green) and depth (blue) directions, resp. The velocity model is indicated for each triplet. Note the greater differences in depth coordinates. (b) Average deviations of origin time with respect to velocity model.

Concluding the localization test, both travel-time residuals and hypocentral shifts indicate a weak preference for the velocity model VOG.

105 **2.2 Test of P-wave polarization**

~~Long-term experience with~~ routine data processing shows that P-wave first-motion polarization of local earthquakes is nearly vertical, regardless of the relatively shallow hypocentres and thus the generally flat rays. This can only be due to the ==pronounced low-velocity surface layer causing the sharp curvature of rays near the surface.== Even though all the tested models are characterized by a positive vertical velocity gradient, the accuracy of modelling the P-wave polarization still 110 remains to be determined.
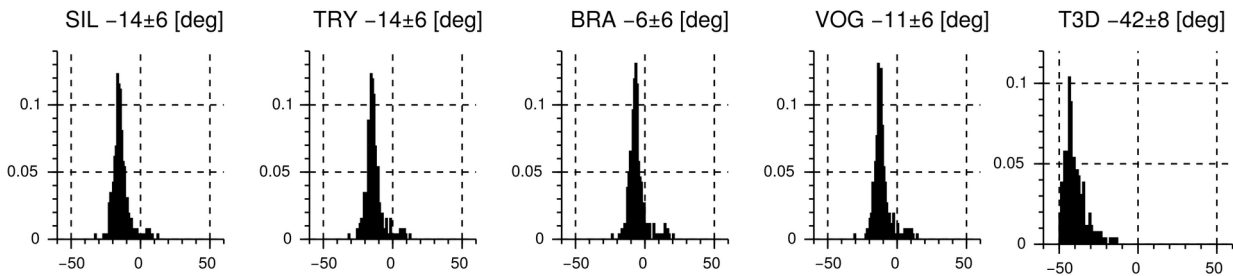
Figure 5. Histograms of differences between observed and calculated incidence angles of the first P-wave motion for all station-earthquake rays with good SNR ratio. The mean value and standard deviation are indicated near the model specification in the title above each histogram.

We compared observed and calculated incidence angles of the first P-wave motion. While evaluating the synthetic P-wave polarization (or similarly the incidence angle and backazimuth)is rather straightforward, having defined the appropriate ray, evaluating the observed incidence angle is slightly complicated, for details see Appendix B. It must be noted here that the observed incidence angle must include a correction for the surface effect (Appendix C).

115 The results are presented in Fig. 5 in the form of histograms calculated separately for each model. As this figure demonstrates, the models are qualitatively equivalent with respect to this test. Histograms of all but T3D models are systematically shifted from the zero position by -6º – -14º and the standard deviation is ~6º, regardless of the model. ~~The model T3D behaves exceptionally,~~ mean residual of the incidence angle is -42º and thus this model is definitely out of consideration for using in methods working with P-wave amplitudes, While the width of the histograms depends mainly on

120 the inaccuracy of real polarizations and thus is model-independent, the bias is mainly caused by imperfections in the velocity model.

~~Let us bear in mind that an incorrect shape of the modelled rays and incorrect polarization may cause problems during some data processing procedures (e.g., moment tensor inversion),~~

2.3 Test of Rayleigh-wave dispersion

125 Málek et al. (2019) published the measurements and processing of distant and ~~local~~ earthquakes recorded by the REYKJANET stations. They obtained a representative Rayleigh-wave phase-velocity dispersion, which was approximated using a rational function with six parameters. The dispersion curve was derived in the period range of 3 s < T < 40 s.

Our models consider a maximum depth of ~10 km, according to the depth distribution of local earthquakes. Consequently, only a part of the Rayleigh-wave phase-velocity curve up to the period ~10 s can be meaningfully confronted with our

130 velocity models. ~~This period-limited dispersion curve to be fitted is shown in Fig. 6. Next,~~ we calculated the Rayleigh-wave phase-velocity dispersion of the fundamental mode for all the tested velocity models in the period range 3 - 10 s. ~~We used~~ the code 'vdisp' developed by Novotný (1999, pers. comm.) which is designed for calculations using 1D layered models

only (Thompson-Haskell formalism is applied, Aki and Richards, 2002). For this purpose, the model T3D was projected onto the 1D depth-only dependent velocity model, allowing for all of the five tested models to be evaluated consistently. ~~The~~

135 ~~results are shown in Fig. 6.~~ Two models, TRY and T3D, are in strong disagreement with the "reference" measurement by Málek et al. (2019). The other three models, SIL, BRA and VOG, coincide well with the reference dispersion. The best fit is provided by models VOG and BRA.

~~If this test were to eliminate inadequate velocity models, TRY and T3D would be removed from consideration. The most preferable models would then be BRA and VOG.~~
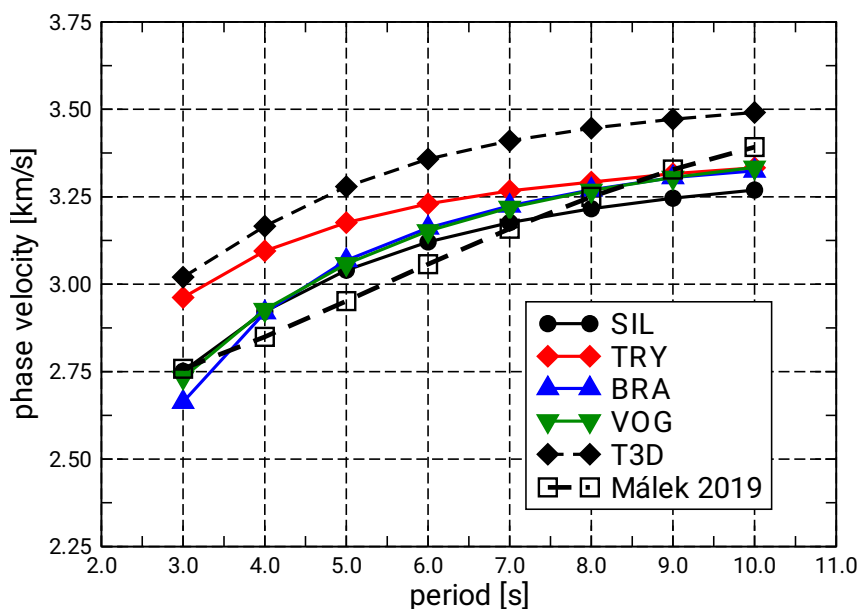

Figure 6. Phase velocity of Rayleigh wave as measured by Málek *et al.* **(2019) and those calculated for the five tested velocity models.**

140 **3 Summary of velocity model testing**

The above performed tests (post-localization residuals, P-wave first motion incidence angles, R-wave dispersion) do not exhibit a strong preference towards ~~one~~ single model. The models can be used more or less interchangeably with virtually the same efficiency. However, at a deeper level, the model TRY ~~could~~ be rejected due to its rather poor agreement between 'observed' and 'predicted' R-wave dispersion. Nevertheless, ~~all~~ the remaining models: SIL, BRA and VOG, could use further

145 improvement. One can speculate about suitable corrections to these models, which would a) decrease travel-time residuals

8

(ideally down to the level provided by the model T3D), b) eliminate the bias between observed and predicted incidence angles (ideally to zero bias) and, c) preserve (or even improve) the fit between 'observed' and 'predicted' R-wave dispersion.

4 Wadati diagrams

When considering any modification of a velocity model, the v_p/v_s ratio introduces an important issue. This parameter is closely related to the rigidity/liquidity of the medium. What is even more significant here is probably not only the absolute value of v_p/v_s, but rather its spatial variation. However, the 1D velocity models studied in this paper can only estimate the depth dependence of v_p/v_s.

In addition to the model testing discussed above, we used a subset of 671 events with at least 10 P and 10 S readings for the determination of v_p/v_s using the method by Wadati (1933). We obtained the mean $v_p/v_s = 1.77 \pm 0.04$. ~~Let us note that~~ this method determines the v_p/v_s averaged along the rays and is exact, provided that the P and S rays travel along the same ray from hypocentre to arbitrary station. ~~For the results see~~ Fig. 7. We also tried to plot the dependence of v_p/v_s on the
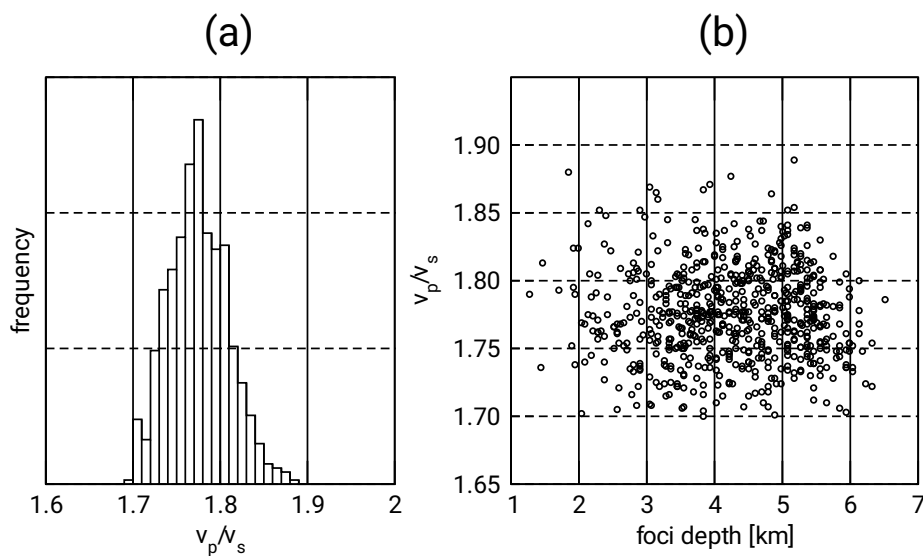

Figure 7. (a) Histogram of the v_p/v_s ratio determined using the Wadati diagram method. Mean value of $v_p/v_s = 1.77$. (b) v_p/v_s as a function of the hypocentre depth.

hypocentre depth, see Fig. 7b. Based on the plot, it appears that v_p/v_s is ~~sufficiently~~ depth-independent.

All four tested 1D velocity models have a depth-independent v_p/v_s ratio, close to the value provided by the Wadati method: SIL: 1.781, TRY: 1.769, BRA: 1.780, VOG = 1.781. All of the values are slightly above the value given by the Wadati method, albeit within the uncertainty interval.

4 Model correction scheme

Our aim was not to construct an entirely new model but rather to propose a small-scale correction to an already existing model in order to improve its performance while retaining the simplicity of the 1D models. Based on the performed tests, it follows that altering the part of the velocity profile near the surface could a) remove the bias seen in incidence angle

165   residuals and, b) if such an alteration were also station-dependent, it could decrease the travel-time residuals, as it would act similarly to station corrections. ~~Moreover, changing the velocity near the surface would not significantly impact the Rayleigh-wave dispersion.~~

The proposed scheme is illustrated in Fig. 8. For each station, two parameters are searched for: v_{opt} and h_{opt}. For depth $h > h_{opt}$, the velocity is unchanged and is the same as in the original model. For velocity at depth $h < h_{opt}$, the original velocity

170   is replaced by a linear function given by two depth-velocity points A, B, where $A = [0, v_{opt}]$ and $B = [h_{opt}, v(h_{opt})]$, so that the
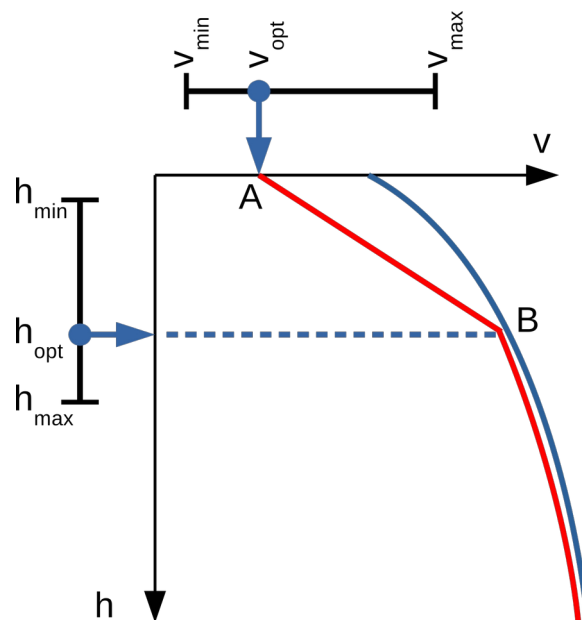

Figure 8. The original 1D velocity model is represented by the blue line. The part between the surface and point B is replaced with line A-B. The corrected model is shown in red.

altered velocity function remains smooth.

The correction scheme is applied to the P-wave velocity model and, when assuming a constant v_p/v_s ratio, the S-wave velocity correction is just a scaled version of that of the P-wave. In conclusion, the problem transforms in finding appropriate doublets of parameters [v_{opt}, h_{opt}] for each station, i.e., having n stations $2n$ parameters are the subject of the search. The

175   criterion for the search is the minimization of the common L2 norm:

$$\Phi = \sum \left(\frac{t_P^{obs} - t_P^{calc}}{\Delta t_P} \right)^2 + \sum \left(\frac{t_S^{obs} - t_S^{calc}}{\Delta t_S} \right)^2 + \sum \left(\frac{inc^{obs} - inc^{calc}}{\Delta inc} \right)^2 + \sum \left(\frac{c^{obs} - c^{calc}}{\Delta c} \right)^2 \quad , \quad (1)$$

$$\boldsymbol{m} = \mathrm{argmin}\,(\Phi), \quad \boldsymbol{m} = \left[[v_{opt} h_{opt}]_1, [v_{opt} h_{opt}]_2, \cdots, [v_{opt} h_{opt}]_n \right]$$

where the first two sums relate to the P- and S-wave travel-time residuals, respectively. The third sum quantifies the disagreement between the P-wave first motion incidence angles and the last sum quantifies the disagreement between the Rayleigh-wave phase velocity dispersion in response to the station-averaged model and the dispersion reported by Málek et

180 al. (2019).

The solution to Eq. 1 was achieved using the Differential Evolution Algorithm (Storn and Price, 1997), i.e., a robust, population-based and non-linear optimizer. The search was arranged in iterative cycles and required hypocentre relocation and ray re-tracing. Ray tracing was accomplished using a simple code that uses 1D model parameters which are selected individually for each station in question. The proposed modelling scheme is thus no longer strictly 1D or 3D, but rather a

185 pseudo-3D model. The algorithm should work well if the hypocentre is below the h_{opt} depth, so that any ray starts in a region with a velocity common for all stations, the only difference being which station is reached from below. Tracing rays from surface sources (e.g., explosions) is ill-advised in such a model, as there is no exact geographical boundary between the neighbouring stations/models.

5 Correcting model VOG

190 The correction scheme ~~can be~~ applied to ~~any of the 1D velocity models discussed above. We decided to illustrate the potential of the correction using~~ the VOG ~~model. This model is weakly favoured over the other models and~~ it is ~~the~~ most ~~widely~~ used model ~~at IG~~, especially for calculating moment tensors.

We selected a subset of 150 well-recorded local events with a maximum number of manual P/S picks and such that their hypocentres were at least 1km apart from each other. A representative data set was thus created with minimum redundancy

195   of nearby foci. In total, we inverted 1422 P-wave picks, 1444 S-wave picks, 483 P-wave first motion incidence angles, and R-wave phase velocities corresponding to only 8 periods (T = 3, 4, ..., 10 s). From these numbers it follows that the inversion result will predominantly reflect the minimization of travel-time residuals, the impact of incidence angle residuals will be lower, and dispersion data will play virtually no role. However, we retained the dispersion data to serve as an independent indicator for signalling situations in which the inversion starts becoming unrealistic. In terms of data space, we worked with

200   a data vector d with dimensions of 1422+1444+483+8 = 3357. Regarding model space m, we worked with 14 stations, resulting in dimensions of 14*2 = 28. From a formal point of view, the inverse problem was strongly overdetermined.
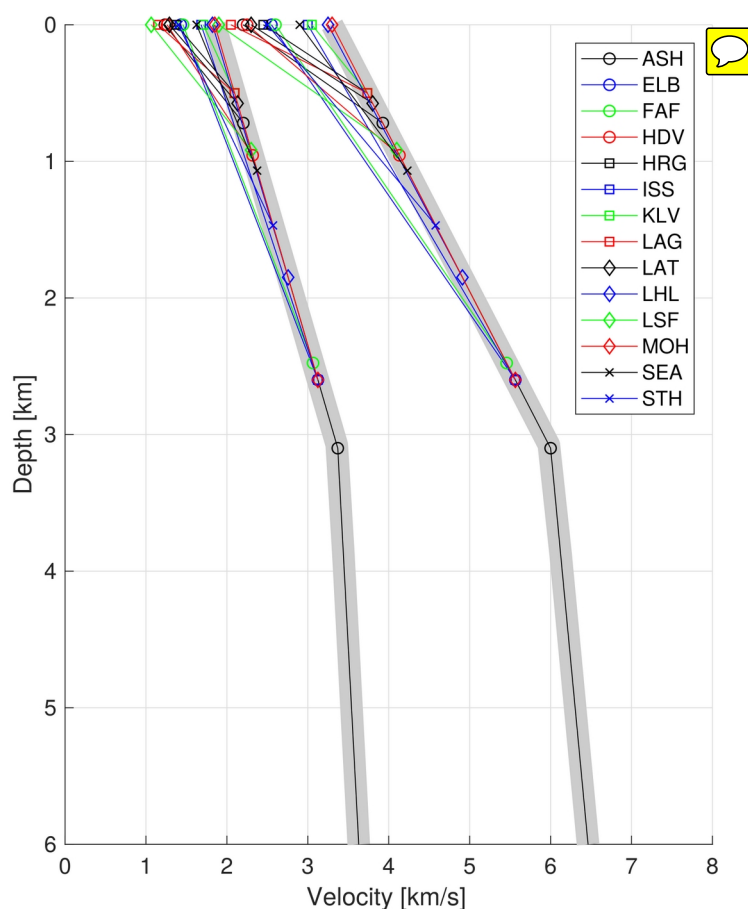

Figure 9. Set of 14 station-dependent 1D velocity models obtained from the correction of the VOG model. The correction applies to the topmost part of the model down to a depth of ~2.5 km. The different models are depicted using different colours and symbols. The default model VOG is shown as a thick grey line in the background.

An important aspect here is the correct weighting of different physical quantities in Eq. 1 (i.e., delta terms). Contrary to the selection of 150 non-collocated events for inversion, we selected as many groups of nearby events as possible and estimated their errors using the scatter of measured quantities within each group: $\Delta t_P = 0.025$ s, $\Delta t_S = 0.040$ s, $\Delta inc = 8°$. The error of the Rayleigh-wave phase velocity was estimated as $\Delta c = 0.1$ km/s by inspecting the scatter of different dispersion curves used for the construction of an average in Málek et al. (2019).

The resulting set of station-dependent 1D velocity models is shown in Fig. 9. The parameters which differentiate the corrected model from the original VOG model are summarized in numerical form in Table 1.

Table 1.

station code	station altitude [m]	v_p [km/s]	v_s [km/s]*	h_{opt} [km]	v_p [km/s]	v_s [km/s]*
		velocities at the surface			velocities at the depth h_{opt}	
ASH	62	2.200	1.233	0.719	3.927	2.203
ELB	121	2.550	1.446	2.600	5.565	3.155
FAF	186	2.600	1.474	2.476	5.457	3.094
HDV	57	2.250	1.276	0.956	4.132	2.342
HRG	200	2.450	1.389	0.500	3.735	2.117
ISS	77	3.000	1.701	2.600	5.565	3.155
KLV	157	3.050	1.729	0.500	3.735	2.117
LAG	18	2.050	1.162	0.500	3.735	2.117
LAT	75	2.300	1.304	0.575	3.801	2.155
LHL	192	3.250	1.842	1.849	4.911	2.784
LSF	44	1.900	1.077	0.917	4.099	2.324
MOH	264	3.300	1.871	2.600	5.565	3.155
SEA	79	2.900	1.644	1.068	4.230	2.398
STH	51	2.500	1.417	1.469	4.579	2.596
* S-wave velocities are P-wave velocities divided by 1.763.						

Note that only the parameters for P-wave model correction were obtained using data inversion, as S-wave model corrections were linked to the P-wave corrections using the standard v_p/v_s ratio equal to 1.763. At stations MOH and LHL, the correction

is almost negligible. At all remaining stations, the correction is more significant. The lowest velocities were found at HDV, LAG and LSF. The thickest correction layer is indicated at stations FAF, ELB and ISS.

6 Efficiency of corrected model VOG

215 We tested the potential of the suggested model correction by repeating the tests documented above for the corrected model VOG (VOGc). There is a collection of histograms in Fig. 10 constructed from a) P-wave travel-time residuals, b) S-wave travel-time residuals and c) P-wave first arrival incidence angles residuals, calculated using the VOG and VOGc models. All of the histograms clearly demonstrate the superiority of VOGc over VOG. The P-wave travel-time residuals dropped from 0.070 s (VOG) to 0.058 s (VOGc), i.e., a 17% reduction was achieved, and in the case of S-wave travel-time residuals there

220 was a decrease from 0.124 s (VOG) to 0.098 s (VOGc), i.e., a 21% reduction was achieved.. For a comparison, see also Fig.
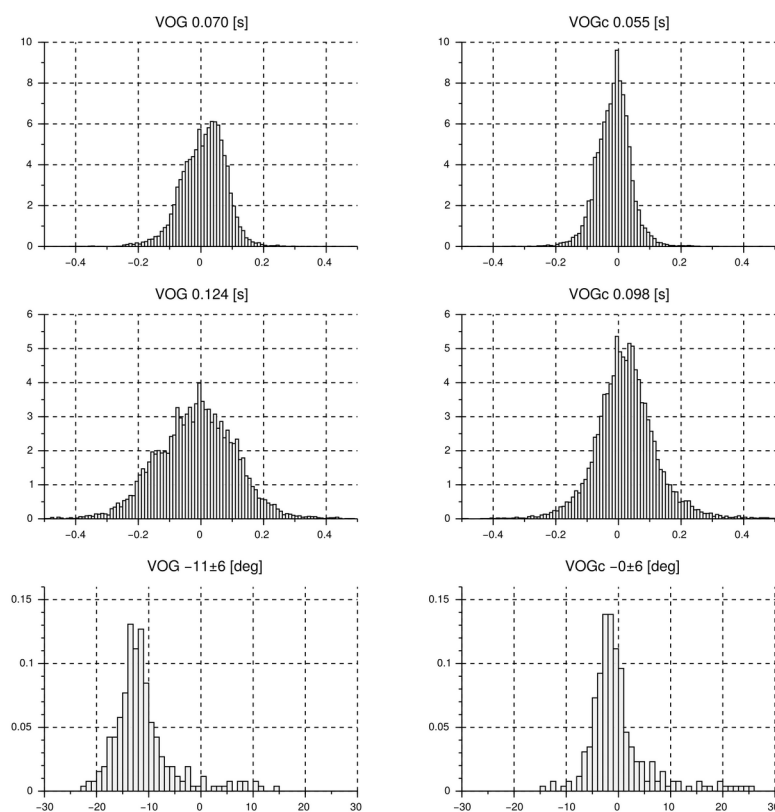

Figure 10. Histograms of residuals between different observed and calculated quantities. The left column depicts histograms calculated in the VOG model, the right column are those calculated in the VOGc model. The top-most row presents P-wave post-localization residuals, the middle row shows S-wave post-localization residuals, and the bottom-most row depicts histograms constructed from observed and calculated incidence angles of the P-wave first motion. The header of each histogram indicates the velocity model (VOG or VOGc) as well as the mean value and standard deviation obtained from the histogram. All histograms are normalized, i.e., the area below the graphs is equal to 1.

3, where the corresponding residuals ⟨⟩e model T3D are 0.062 s and 0.084 s for P- and S-wave, respectively. The model VOGc is thus fully competitive with the model T3D, though it is much more straightforward, using a much lower number of parameters and very simple 1D ray-tracing schemes. In addition, histograms that characterize the incidence angles can also be found in Fig. 10. This produces a slightly different situation, as the standard deviation is the same for both models (9°) but the bias is almost entirely removed in VOGc (the VOG histogram is centred around ~-11°, VOGc is centred around ~0°). The standard deviation is predominantly given by the inaccuracy of measuring the incidence angles and is therefore data-dependent. The bias is predominantly given by how correctly the rays are modelled, i.e., it is model-dependent. From this point of view, VOGc also performs well. The systematically shifted calculated incidence angles may cause problems in situations where P-wave amplitudes are being analysed (e.g., moment tensor solutions).

We also tested the differences between VOG and VOGc in terms of the Rayleigh-wave dispersion. This criterion is of minor
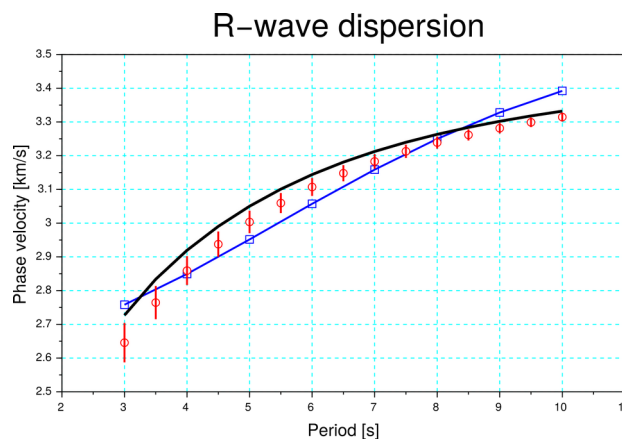

Figure 11. The blue line with squares represents the dispersion as reported by Málek *et al.* (2019). The black line is the dispersion predicted by the VOG model. The red circles show the dispersion predicted and averaged over 14 station-dependent models constituting VOGc. The vertical red bars that intersect the red circles are standard deviations of the VOGc dispersion. Generally, the red symbols are closer to the blue line than the black line is to the blue one.

importance and is used only as a qualitative indicator of the inversion. However, even this test prefers VOGc over VOG. Since VOGc is constituted as a set of 14 station-dependent 1D models, we performed 14 calculations of Rayleigh-wave phase velocity dispersion and estimated their mean and standard deviation using this dataset. The results are depicted in Fig. 11. While the overall agreement with the dispersion reported by Málek et al. (2019) may be questionable, it is better than that of VOG; the only example of VOG predicting dispersion more consistently with Málek's dispersion than VOGc is for the period T = 3 s. Let us note that this period is the lowest period for which the reference data was calculated and may not be well determined. It is evident that Málek's model may not perfectly reflect near-surface properties of the medium.

7 Several features of model VOGc

The localization of earthquake hypocentres using either the VOG or VOGc model produces two different hypocentre sets.

240 Hypocentre coordinates (or their pair-wise differences) are not a salient measure for determining the more preferable model..
However, the impact of the model on the localization results could be of interest here. When comparing VOG to VOGc, the movement of the corresponding hypocentres is not very significant. The mean shift in the E-W direction is 0.111 km towards the East, the mean shift in the N-S direction is 0.018 km towards the North; the biggest change is in the depth, as VOGc hypocentres are on average 0.197 km deeper. Even the seismicity pattern, indicated in Fig. 1 (only a superficial illustration),
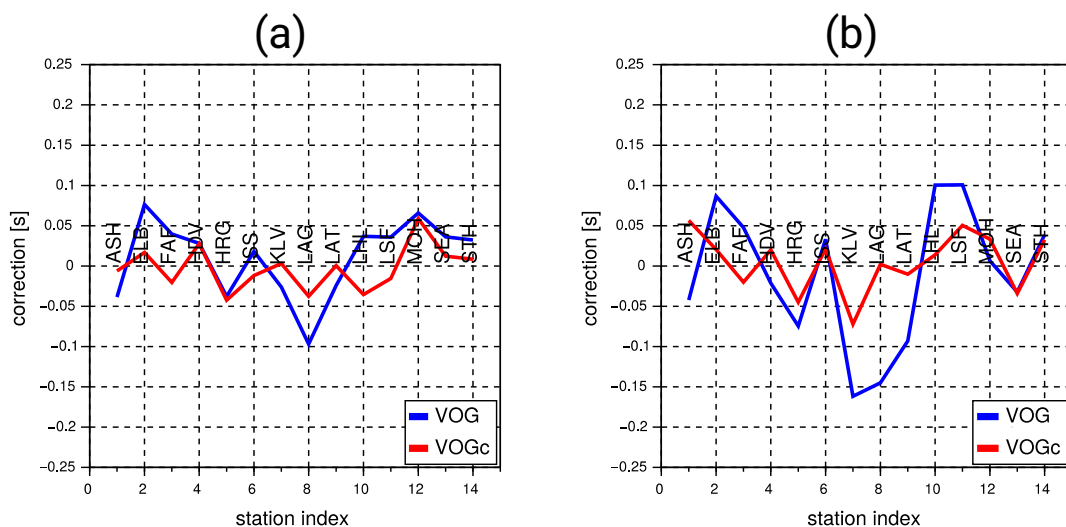

Figure 12. (a) P-wave and (b) S-wave station corrections calculated in the VOG and VOGc models. Note that VOGc corrections are significantly smaller than the VOG corrections.

245 remains nearly the same. As the two models, VOG and VOGc, differ only in parts close to the surface, the application of VOGc may be similar to the application of station corrections in VOG. This can be evidenced by Fig. 12. The station corrections in the model VOGc are much lower than those of model VOG. The VOGc model thus absorbs station-dependent travel-time anomalies similarly to the application of station corrections. The key difference is that the rays in VOGc differ from those in VOG and that modelling a different ray-dependent seismological problem may yield more precise results.

250 The sparse station configuration with a typical inter-station distance of ~10 km does not allow for any geological implications based on, e.g., the surface vertical velocity gradient or the depth of the top-most layer. However, one interesting feature is the positive correlation of the surface velocity and the station altitude, Fig. 13. We explain this feature by altitude-dependent age or by the altitude-dependent weathering of the lava rocks (the latter rests on the precondition that more resistant rocks form hills and vice versa).
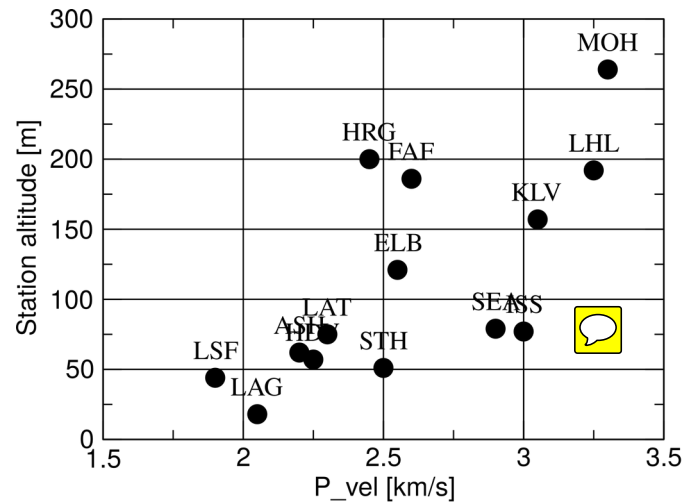
Figure 13. Surface P-wave velocity at different stations shown together with the station altitude. There is a clear positive correlation between these two parameters.

8 Conclusions

In order to classify the suitability of several published 1D velocity models, we performed a series of tests to quantify the performance of the models. We tested the post-localization residuals, mutual movement of hypocentres, residuals between measured and model-predicted P-wave first-motion incidence angles, and the qualitative agreement between model-predicted and reported Rayleigh-wave phase velocity. The results of the individual tests are not always coherent across the models. In summary, the tested 1D velocity models:

- provide more or less comparable travel-time residuals;
- provide more or less identical epicentres of earthquakes, with larger differences observed for depth. The hypocentre depths in the models SIL, TRY and BRA exhibit the largest differences from one another;
- demonstrate the necessity of including a low-velocity surface layer below each station to correctly meet the P-wave polarization, which hopefully helps to decrease the travel-time residuals at the same time;
- predict R-wave dispersion, which excludes the model TRY from consideration.

There is no strong preference for any one model in particular, though the model VOG seems to be the best candidate for further tuning and correction.

Based on the argumentation above, we decided to modify the 1D model, VOG, into a pseudo-3D model, VOGc. The modification involved the inclusion of a surface layer with a vertical velocity gradient below each station involved. The parameters of the layers were calculated using data inversion. The inversion process comprised only the P-wave model, as the S-wave model is a scaled version of the P-wave model based on the predefined v_p/v_s ratio. Inversion is performed to minimize the norm of the residuals of travel-times, P-wave incidence angles and Rayleigh-wave phase-velocity dispersion.

17

The result is a set of 1D velocity models, each one valid for one particular station. Ray tracing can still be accomplished using a 1D approach, which remains the quickest and easiest option. The pseudo-3D model VOGc is defined by fewer parameters than any fully 3D model. The inevitable drawback of such an approach is that only rays from hypocentres deeper than the deepest surface layer can be modelled correctly. After the construction of the model VOGc and subsequent testing, we can conclude that

- post-localization travel-time residuals dropped to a level comparable with those provided by the true 3D model T3D;
- P-wave first-motion incidence angles have zero bias;
- independently measured R-wave phase-velocity dispersion is acceptably met.

We propose the corrected model to be used for the routine processing of REYKJANET data. Nevertheless, the further development of 3D models is by no means called into question, as such methods are still the only viable option for discovering e.g., the geological structure.

Acknowledgements

Code/Data availability

The data is embargoed according to the license terms until April 2026. After this period, it will be available at https://doi.org/10.7914/SN/7E_2013. The calculations were carried out using a script in MATLAB, which can be freely obtained via email b.ruzek@ig.cas.cz

Authors contribution

The authors shared the work equally, i.e. their contribution is 1/3, 1/3, 1/3.

Competing interests

There are no competing interests for the authors of the text.

References

Aki, K. and Richards, P. G.: Quantitative Seismology. University Science Book, 2nd ed., Sausalito, CA 94965, 2002.

Bjarnason, I. Th., Menke, W., Flóvenz, Ó. G. and Caress, D.: Tomographic image of the Mid-Atlantic Plate Boundary in southwestern Iceland. *J. Geophys. Res*., **98**, (B4), 1993.

Brandsdóttir, B. and Menke, W.H.: The seismic structure of Iceland, *Jökull 58*, 17-34, 2008.

Geoffroy, L. and Dorbath, C.: Deep downward fluid percolation driven by localized crust dilatation in Iceland, *Geophys. Res. Lett*., **35**, L17302, 1-6, https://doi.org/10.1029/2008GL034514, 2008.

Greenfield, T., White, R.S. and Roecker, S.: The magmatic plumbing system of the Askja central volcano, Iceland, as imaged by seismic tomography, *J. Geophys. Res*. Solid Earth, **121**, 7211-7229, https://doi.org/10.1002/2016JB013163, 2016.

Jakoubková, H.: Earthquake swarms in diverse tectonic environments: West Bohemia and Southwest Iceland, *Doctoral thesis*, *Faculty of Mathematics and Physics, Charles University, Prague*. Available in electronic form at https://geo.mff.cuni.cz/theses/2018-Jakoubkova-PhD.pdf, 2018.

Jousset, P., Blanck, H., Franke, S., Metz, M., Águstsson, K., Verdel, A., and Flovenz, O. G.: Seismic Tomography in Reykjanes, SW Iceland. *In European geothermal congress 2016*: Strasbourg, France, 2016.

Lomax, A., Michelini, A. and Curtis, A.: Earthquake Location, Direct, Global-Search Methods, in Encyclopedia of Complexity and System Science, Part 5, Meyers, R. A. (ed.), Springer, New York, 2449-2473, https://doi.org/10.1007/978-0-387-30440-3, 2009.

Málek, J., Brokešová, J. and Novotný, O.: Seismic structure beneath the Reykjanes Peninsula, southwest Iceland, inferred from array-derived Rayleigh wave dispersion, *Tectonophysics*, **753**, 1-14, https://doi.org/10.1016/j.tecto.2018.12.020, 2019.

Mitchell, M.A., White, R.S., Roecker, S. and Greenfield, T.: Tomographic image of melt storage beneath Askja Volcano, Iceland using local microseismicity, *Geophys. Res. Lett*., **40**, 5040-5046, https://doi.org/10.1002/grl.50899, 2013.

Růžek, B.: Seismic anisotropy in the rift of the Reykjanes Peninsula, SW Iceland, calculated using a new tomographic method. *Pure and Applied Geophysics*, **178** (8), 2871-2903, https://doi.org/10.1007/s00024-021-02784-1, 2021.

Storn R. and Price K.: Differential Evolution – A simple and efficient heuristic for global optimization over continuous spaces. *J. Glob. Optim.*, **11**, 241-354, 1997.

Tryggvason, A., Rögnvaldsson, S. T. and Flóvenz, Ó. G.: Three-dimensional imaging of the P- and S-wave velocity structure and earthquake locations beneath Southwest Iceland. *Geophys. J. Int.*, **151**, 848-866, https://doi.org/10.1046/j.1365-246X.2002.01812.x, 2002.

Vogfjörd, K. S., Nolet, G., Morgan, W. J., Allen, R. M., Slunga, R., Bergsson, B. H., Erlendsson, P., Foulger, G., Jakobsdóttir, S. S., Julian, B., Pritchard, M. and Ragnarsson, S.: Crustal profiling in Iceland using earthquake source arrays. *AGU Fall meeting*, *Abstract S61C-1161*, San Francisco, California, 6-10 December, 2002.

Wadati, K., 1933. On the travel time of earthquake waves. Part II, *Geophys. Mag*. **7**, 101-111.

Weir, N. R. W., White, R. S., Brandsdóttir, B., Einarsson, P., Shimamura, H. and Shiobara, H.: Crustal structure of the northern Reykjanes Ridge and Reykjanes Peninsula, southwest Iceland. *J. Geoph. Res.: Solid Earth*, **106** (B4), 6347-6368, 2001.

335   www2023a: http://www.fdsn.org/networks/detail/7E_2013/

www2023b: https://github.com/alomax

20

Appendix A. Numerical specification of the velocity models

All models are specified in the format required by the NonLinLoc software.

LAYER, depth, Vp_top, Vp_grad, Vs_top, Vs_grad, p_top, p_grad

340   (Note: The last two columns relate to density. These values are of formal significance only).

Model BRA

LAYER	0.00	2.80	1.333	1.57	0.749	2.7	0.0
LAYER	0.15	3.00	1.429	1.69	0.803	2.7	0.0
LAYER	0.50	3.50	0.700	1.97	0.393	2.7	0.0
LAYER	1.00	3.85	1.100	2.16	0.618	2.7	0.0
LAYER	1.50	4.40	0.800	2.47	0.449	2.7	0.0
LAYER	2.00	4.80	1.000	2.70	0.562	2.7	0.0
LAYER	2.50	5.30	0.700	2.98	0.393	2.7	0.0
LAYER	3.00	5.65	0.700	3.17	0.393	2.7	0.0
LAYER	3.50	6.00	0.600	3.37	0.337	2.7	0.0
LAYER	4.00	6.30	0.430	3.54	0.242	2.7	0.0
LAYER	5.00	6.73	0.050	3.78	0.028	2.7	0.0
LAYER	6.00	6.78	0.070	3.81	0.039	2.7	0.0
LAYER	7.00	6.85	0.050	3.85	0.028	2.7	0.0
LAYER	8.00	6.90	0.040	3.88	0.022	2.7	0.0
LAYER	10.0	6.98	0.038	3.92	0.021	2.7	0.0
LAYER	13.2	7.10	0.000	3.99	0.000	2.7	0.0

Model SIL

LAYER	0.00	3.53	0.940	1.98	0.530	2.7	0.0
LAYER	1.00	4.47	0.690	2.51	0.390	2.7	0.0
LAYER	2.00	5.16	0.440	2.90	0.250	2.7	0.0
LAYER	3.00	5.60	0.360	3.15	0.200	2.7	0.0

LAYER	4.00	5.96	0.260	3.35	0.140	2.7	0.0
LAYER	5.00	6.22	0.280	3.49	0.160	2.7	0.0
LAYER	6.00	6.50	0.100	3.65	0.060	2.7	0.0
LAYER	7.00	6.60	0.060	3.71	0.030	2.7	0.0
LAYER	8.00	6.66	0.070	3.74	0.040	2.7	0.0
LAYER	9.00	6.73	0.045	3.78	0.025	2.7	0.0
LAYER	15.0	7.00	0.040	3.93	0.022	2.7	0.0
LAYER	20.0		0.017	4.04	0.010	2.7	0.0
LAYER	32.0	7.40	0.000	4.16	0.000	2.7	0.0

345

Model TRY

LAYER	0.00	3.60	1.100	2.05	0.600	2.7	0.0
LAYER	1.00	4.70	0.900	2.65	0.500	2.7	0.0
LAYER	2.00	5.60	0.500	3.15	0.300	2.7	0.0
LAYER	3.00	6.10	0.300	3.45	0.150	2.7	0.0
LAYER	4.00	6.40	0.100	3.60	0.050	2.7	0.0
LAYER	5.00	6.50	0.100	3.65	0.100	2.7	0.0
LAYER	6.00	6.60	0.033	3.75	0.017	2.7	0.0
LAYER	9.00	6.70	0.020	3.80	0.010	2.7	0.0
LAYER	14.0	6.80	0.100	3.85	0.050	2.7	0.0
LAYER	15.0	6.90	0.100	3.90	0.050	2.7	0.0
LAYER	16.0	7.00	0.014	3.95	0.007	2.7	0.0
LAYER	23.0	7.10	0.100	4.00	0.050	2.7	0.0
LAYER	24.0	7.20	0.200	4.05	0.150	2.7	0.0
LAYER	25.0	7.40	0.000	4.20	0.000	2.7	0.0
LAYER	32.0	7.40	0.000	4.20	0.000	2.7	0.0

Model VOG

LAYER	0.00	3.30	0.871	1.85	0.489	2.7	0.0

LAYER	3.10	6.00	0.183	3.37	0.104	2.7	0.0
LAYER	8.00	6.90	0.033	3.88	0.019	2.7	0.0
LAYER	17.0	7.20	1.500	4.04	0.843	2.7	0.0
LAYER	17.2	7.50	0.055	4.21	0.031	2.7	0.0
LAYER	19.0	7.60	0.008	4.27	0.005	2.7	0.0
LAYER	25.0	7.65	0.010	4.30	0.006	2.7	0.0
LAYER	35.0	7.75	0.000	4.35	0.000	2.7	0.0

350 **Appendix B. Calculation of polarization angles**

Calculating the P-wave polarization may be somewhat tricky in reality. The seismograms of local earthquakes recorded by REYKJANET stations do not present single P- and S-wave pulses. Instead, they depict complex and relatively intense scattered waveform arrivals from which no isolated phases can be easily separated. The particle motion of a P wave is thus typically a complex curved path in which the dominant direction often changes. The only option for estimating the true polarization of a

355 direct P wave is to only follow the particle motion of a short time segment just after the first P-wave onset. Due to the sheer quantity of data, only an automated approach is feasible here. Our procedure consists of the following steps, the parameters of which were set up more or less empirically:

1. Seismograms are high-pass filtered using the Butterworth filter of 3rd order with f_c = 5 Hz.

2. Three waveform segments [z, n, e] the length τ of which is four samples (τ = 16 ms) starting immediately after the
360   P-wave onset are selected.

3. The offset of waveform segments is removed: $z \rightarrow z$ - mean(z), $n \rightarrow n$ - mean(n), $e \rightarrow e$ - mean(e).

4. The matrix $\boldsymbol{P}$ is created whose columns are [z, n, e].

5. Singular vectors and singular numbers of $\boldsymbol{P}$ using the *svd* procedure are calculated:

$$[\boldsymbol{U}, \boldsymbol{S}, \boldsymbol{V}] = svd(\boldsymbol{P}) \tag{A-1}$$

365 6. First column $\boldsymbol{v}$ of the matrix $\boldsymbol{V}$ corresponds to the maximum linear-like motion and is identified with the potential P-wave polarization. The degree of linearity r is defined as the ratio between the largest and middle singular number:

$$r = \frac{s_1}{s_2}, s_k = \boldsymbol{S}_{kk} \quad . \tag{A-2}$$

7. The procedure is repeated from step 3 with one sample longer seismogram segments [z, n, e], until the linearity term r decreases.

370 8. Final polarization is normalised, i.e. $\boldsymbol{v} \rightarrow \boldsymbol{v}/norm(\boldsymbol{v})$ and, optionally multiplied by -1 in order to obtain negative $\boldsymbol{v}_1$ component (i.e. the vertical movement is a priori assumed to be downwards) which corresponds to the station-to-focus direction.

9. Incidence angle i is given by

$$i = \arcsin(|v_1|) \tag{A-3}$$

375 *Note*: Seismograms can be integrated in order to obtain displacement recordings, which are closely linked to polarization. However testing this option did not produce any improvements and, the results were even more scattered than if using original velocity recordings.

24

Appendix C. Apparent and true ray incidence angle

Due to the interference of the incoming P-wave and P and S waves reflected from the Earth's surface, the measured

380 polarization as given above does not express exactly polarization of the incoming P-wave which is the measurement of

interest here. The amplification of the vertical and horizontal components is different due to the Earth's surface. Let us say

the P-wave is propagating upwards and its true unit polarization vector is $\boldsymbol{p} = (p_x, p_y, p_z)$. The medium is considered

homogeneous isotropic with velocities v_P and v_S. In this case the amplification factors are

$$gain_{Pz} = \frac{2 * v_P}{v_S^2} * \frac{C_i * aux}{D}$$
$$gain_{Ph} = \frac{4 * v_P * p_h}{v_S^2} * \frac{C_i * C_j}{D} \qquad , \tag{B-1}$$

385 where

$$p_h = \frac{\sqrt{p_x^2 + p_y^2}}{v_P}$$

$$C_i = \sqrt{\frac{1}{v_P^2} - p_h^2}$$

$$C_j = \sqrt{\frac{1}{v_S^2} - p_h^2} \qquad . \tag{B-2}$$

$$aux = \frac{1}{v_S^2} - 2 * p_h^2$$

$$D = aux^2 + 4 * p_h^2 * C_i * C_j$$

Once we know $\boldsymbol{p}$ and the v_P and v_S velocities, the true polarization vector is modified to the apparent (observed) polarization

vector $\boldsymbol{p}^{obs}$

$$\boldsymbol{p}^{obs} = \left(p_1 * gain_{Ph}, p_2 * gain_{Ph}, p_3 * gain_{Pz} \right) \quad . \tag{B-3}$$
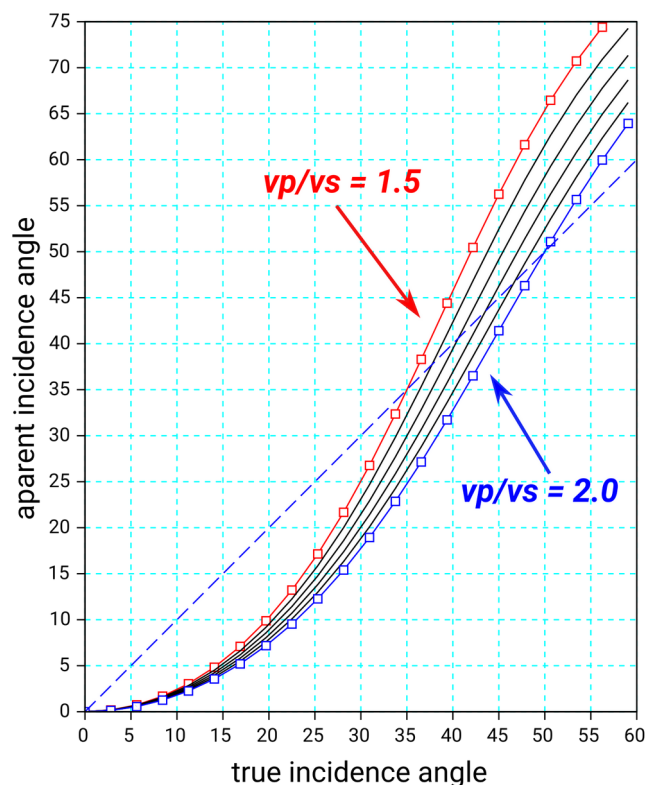
390 For detailed derivation see Aki and Richards (1980).

Figure C1. Graphs showing the relation between the true and apparent incident angles of the P wave. The curves are calculated for different vp-to-vs ratios in the range between 1.5 and 2.0 with a step of 0.1. The "standard" medium with a v_p/v_s ratio equal to sqrt(3) is in close proximity to the central curve. For typical rays that cross the low-velocity layer near the surface, the apparent incidence angle will be around 5º, while the true incidence angle should be around 15º, with only a weak dependence on the v_p/v_s ratio. The dashed blue line is the y=x line for ease of navigating the sign of the angular correction. Real angular correction (apparent → true) is calculated numerically by an interpolation technique using these curves.